Journal of Colloid and Interface Science 553 (2019) 682–687

Contents lists available at ScienceDirect

Journal of Colloid and Interface Science

journal homepage: www.elsevier.com/locate/jcis

Regular Article

Tunneling of photon-generated carrier in the interface barrier induced resistive switching memory behaviour

Bai Sun [a,*], Tao Guo [b], Guangdong Zhou [c], Shubham Ranjan [d], Wentao Hou [e], Yunming Hou [f], Yong Zhao [a,*]

[a] College of Physics and Energy, Fujian Normal University, Fuzhou 350117, China
[b] State Key Laboratory of Applied Optics, Changchun Institute of Optics and Fine Mechanics, Chinese Academy of Sciences, Changchun 130033, China
[c] Institute for Clean Energy & Advanced Materials (ICEAM), Southwest University, Chongqing 400715, China
[d] Department of Electrical and Computer Engineering, University of Waterloo, Waterloo, Ontario N2L 3G1, Canada
[e] College of Materials Science and Technology, Nanjing University of Aeronautics and Astronautics (NUAA), Yudao Street 29, 210016 Nanjing, China
[f] Oil Testing and Perforating Company of Daqing Oilfield Limited Company, Daqing, Heilongjiang 163000, China

GRAPHICAL ABSTRACT

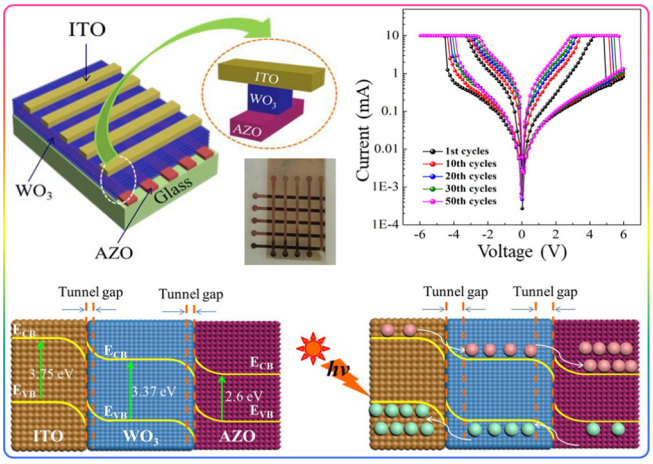

ARTICLE INFO

Article history:
Received 27 April 2019
Revised 5 June 2019
Accepted 23 June 2019
Available online 24 June 2019

Keywords:
Resistive switching
Tunneling
Photon-generated carrier
Schottky barrier
Memory device

ABSTRACT

The resistive switching effect is a great physical phenomenon that the resistance of a material can be reversibly changed by applying an electric pulse, which is useful to constructing the nonvolatile resistance random access memory (RRAM) in the next generation of memory system. In this work, a sandwich structure (ITO/WO_3/AZO) was prepared by using WO_3 film (~300 nm) as the dielectric layer meanwhile indium tin oxide (ITO) as the top electrode and aluminium-doped zinc oxide (AZO) as the bottom electrode. An enhanced resistive switching memory behavior was observed in the sample processed by light-illumination. Furthermore, the set voltage (V_{set}) and reset voltage (V_{reset}) are increased but the HRS/LRS resistance ratio is decreased with the increasing of illumination time for 600 °C annealed sample. Through further analysis, a physical model on the tunneling of photon-generated carrier in the Schottky barrier layer driven by electric pulse is proposed to explain the enhanced resistive switching

* Corresponding authors.
E-mail addresses: sunbai2010@163.com (B. Sun), yzhao@swjtu.edu.cn (Y. Zhao).

https://doi.org/10.1016/j.jcis.2019.06.076

memory behavior. The suggested mechanism is highly pivotal for the resistive switching phenomenon to be properly applied in the nonvolatile RRAM device.

1. Introduction

With the continuous progress of material science and the rapid development of semiconductor device fabrication technology, the size of semiconductor electronic devices has been continuously reduced to nanometer size [1,2]. In particular, the size of memory devices is getting smaller and smaller, and the storage density is constantly getting higher [3]. However, the traditional memory devices, such as magnetic memory, flash and ferroelectric memory, could gradually no longer meet the needs of new information technology because they have size constraints and cannot indefinitely reduce the size of device [4]. Therefore, it is necessary to develop new types of memory devices. Among the new concept memory technology, the most promising one is the resistance random access memory (RRAM) based on the resistive switching effect [5–7]. The RRAM has many advantages [8], such as the ability to be manufactured in to nano-scale, the high storage density, the simple device structure, the fast reading and writing speed, the low energy consumption, and the possibility to be extended to neuromorphic applications [9,10]. Therefore, it is very significant to promote the research of resistive switching memory [11].

At present, the research of resistive switching behaviour has aroused the interest of many scientists [12]. The resistive switching phenomenon has been observed in many materials, such as metal oxides, semiconductors, organic materials and biomaterials, and so on [2,13–15]. However, up to now, the physical mechanism of the resistive switching effect has not been fully revealed, which limits the process of the RRAM commercialization to a certain extent [16]. In addition, with the rapid development of information technology, the research of multistate memory has been paid more and more attention [17]. The light signal and electrical pulse are the most suitable matching because of the light-electron double controlled resistive switching memories has been widely reported [18–20]. Indeed, the light is also a kind of electromagnetic wave, and its transmission is not subject to distance [21]. Therefore, the light-electron double controlled RRAM should have very important potential application [22].

In previous reports, it was considered that tungsten trioxide (WO_3) is a unique *n*-type semiconductor material with a band gap of about 2.7 eV and high solar absorption efficiency [23]. It shows excellent properties in photocatalysis, electrochromism, photochromism and gas chromism [24–27]. Therefore, WO_3 is widely used in discoloration devices, solar energy devices, sensors, photoelectrochemical devices, and so on.

In this work, the WO_3 film with thickness of ~300 nm was deposited as the functional layer to construct the resistive switching memory device, in which the ITO and AZO were selected as the top and bottom electrode, respectively. Furthermore, the enhanced resistive switching memory behaviour is observed after the sample was annealed at 600 °C and then illuminated by white-light. In addition, the V_{set} and V_{reset} are increased but the HRS/LRS resistance ratio is decreased with the increasing of illumination time for the 600 °C annealed sample. Finally, a physical model on the tunnelling of photon-generated carrier inside the Schottky barrier layer is suggested to explain the resistive switching memory behaviour.

2. Materials and methods

In our experimental process, a magnetron sputtering system was mainly used to prepare the resistive switching device. Firstly, an AZO film (~500 nm) is deposited onto a glass substrate as the bottom electrode by using a metal mask with a slit size of ~500 μm. Next, a WO_3 film with a thickness of approximately 300 nm was grown onto the bottom electrode AZO. Finally, the top electrode ITO was deposited onto the WO_3 film by using same mask perpendicular to the bottom electrode. The as-fabricated device is shown in Fig. 1(a), and it is obvious that the device is three-decker with a sandwich structure.

The cross-sectional morphology of the device is observed using a scanning electron microscope (SEM), and the energy dispersive X-ray spectroscopy (EDS) was used to confirm the element composition in the sample. The X-ray diffraction (XRD) was used to confirm the phase composition of the sample. The visible absorption spectra were characterized by ultraviolet–visible spectrophotometer. The sample was heat treated in a tubular furnace filled with nitrogen (N_2), and the light source used in the experiment is a solar simulator. The electrical performance of the device is characterized by an electrochemical workstation.

3. Results and discussions

The schematic chart of as-prepared device is shown in Fig. 1(a), in which we can see the device has a crossbar structure. Fig. 1(b) shows the cross-sectional SEM image of as-prepared device with ITO/WO_3/AZO structure, it can be observed that the thickness of WO_3 film layer is ~300 nm, which is sandwiched in the between the top electrode ITO and bottom electrode AZO. In order to confirm the purity of WO_3 active layer, the as-prepared WO_3 film was characterized by EDX. It indicated that the active layer only contains O and W. And other impurity elements were not found. The inset of Fig. 1(c) exhibits a photograph of device, in which each junction of top and bottom electrodes is a resistive switching cell. The XRD pattern of as-deposited WO_3 film is displayed in Fig. 1(d), which is consistent with the reported result of the previous literature [28], and these diffraction peaks are obviously sharp, suggesting good crystallinity.

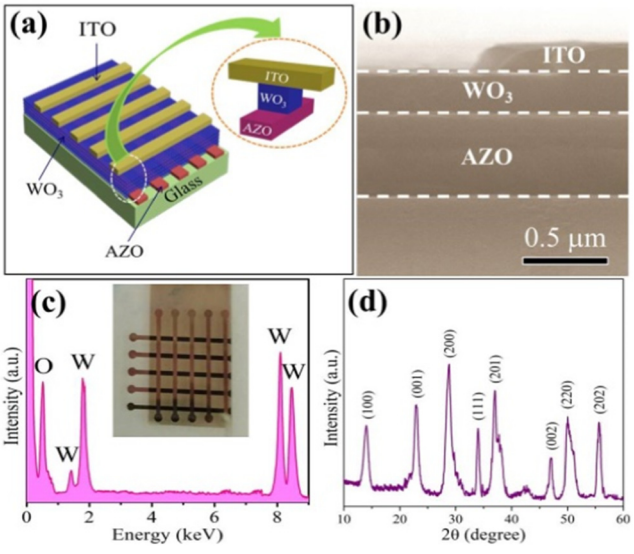

Fig. 1. (a) Schematic chart of as-prepared device with ITO/WO_3/AZO sandwich structure. (b) The cross-sectional SEM image of device. (c) The EDS of WO_3 film; the inset shows the photograph of as-prepared device. (d) The XRD spectra of WO_3 film.

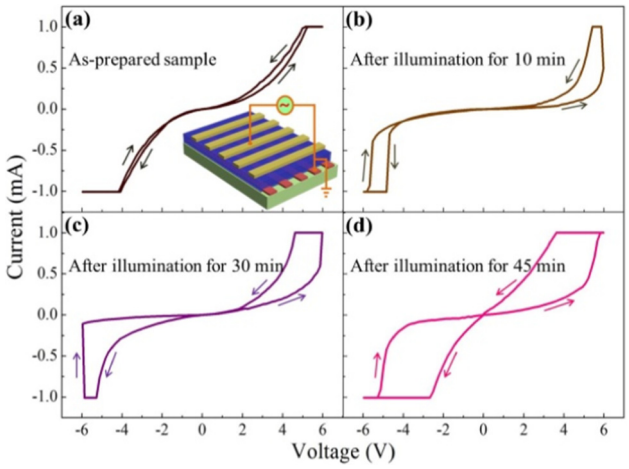

Fig. 2. The I-V curves were tested after the sample was light-illuminated for different time.

The test circuit diagram is shown in the inset of Fig. 2(a). Here, the resistive switching memory effect was tested after the sample was illuminated for different time using white-light with the power density ~50 mW/cm^2. It can be found that the I-V hysteretic loop is very unconspicuous for the as-prepared sample without illumination from Fig. 2(a), in which these arrows in the figure represent the direction of the external voltage cycle scan. We can observe the I-V hysteretic loop become obvious after the device was exposed in illumination for 10 min in Fig. 2(b). Further, we increased the light-illumination time to 30 min, the I-V curve with a lager loop was observed in Fig. 2(c). Finally, the resistive switching memory window can be achieved to largest for the device with the light-illumination time of 45 min, as shown in Fig. 2(d). The above results indicate the resistive switching effect of WO_3 film can be enhanced by increasing light-illumination time.

In order to understand the effect of light-illumination on resistive switching memory behaviour, the change of HRS/LRS resistance ratio with the light-illumination time is draw in Fig. 3 under the read voltage of 3.0 V, we can see that the HRS/LRS resistance ratio is ~1.7 for the as-prepared sample without illumination but it can be increased to ~2.2 after the device was irradiated for 10 min. If we continuously increase the light-illumination time to 30 min, the HRS/LRS resistance ratio can be increased to ~4.3. In particular, the largest HRS/LRS resistance ratio of ~7.5 can be reached after the sample was irradiated for 45 min. The above data indicate the light-illumination time can enlarge the HRS/LRS resistance ratio (memory window), which is very important for high memory density RRAM applications [29].

Further, the resistive switching memory effect is tested after the sample was firstly annealed at 600 °C and then illuminated for different time. It is still found that the I-V hysteretic loop is more and more obvious with increasing of illumination time, as shown in Fig. 4. These data similarly suggest the resistive switching effect can be increased by increasing of light-illumination time.

The change of HRS/LRS resistance ratio with the light-illumination time for these samples annealed at 600 °C is shown in Fig. 5. It can be observed the HRS/LRS resistance ratio can be enlarged after these samples were annealed at 600 °C. Obviously, the largest HRS/LRS resistance ratio of ~9.5 can be realized after the sample was irradiated for 45 min and annealed at 600 °C, which suggests the light-illumination time and appropriate heat treatment can collectively enlarge the HRS/LRS resistance ratio. Larger HRS/LRS resistance ratio is very significant for RRAM applications [30].

Fig. 6(a) shows the I-V curves of continuous 50 cycles after the sample was firstly annealed at 600 °C and then irradiated for 30 min, in which we can see that the loop is continuously increased with the cycle times. The corresponding I-V curves in the logarithmic form are exhibited in Fig. 6(b). We can find the range of V_{set} voltage is from 4.85 V to 5.78 V from Fig. 7(a), and the V_{rest} voltage

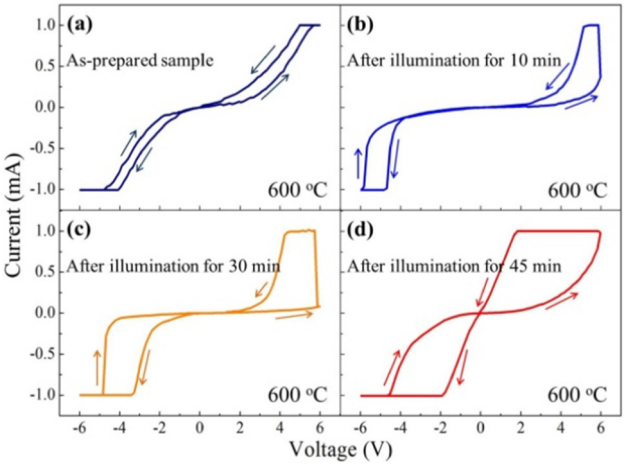

Fig. 4. The I-V curves were tested after the sample was firstly annealed at 600 °C and then illuminated for different time.

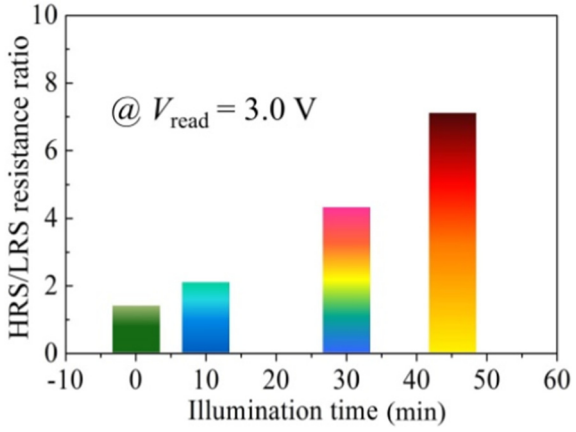

Fig. 3. The change of HRS/LRS resistance ratio with the light-illumination time.

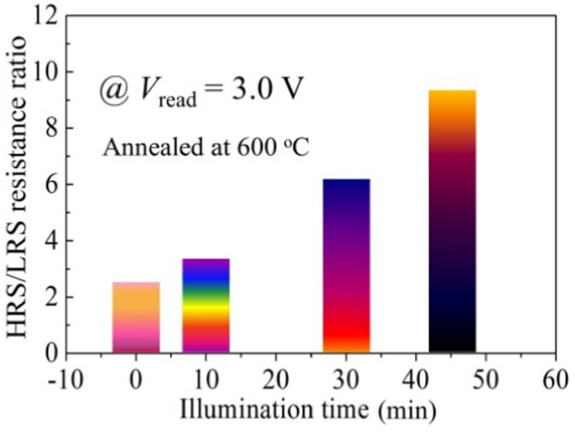

Fig. 5. The change of HRS/LRS resistance ratio with the light-illumination time for the sample annealed at 600 °C.

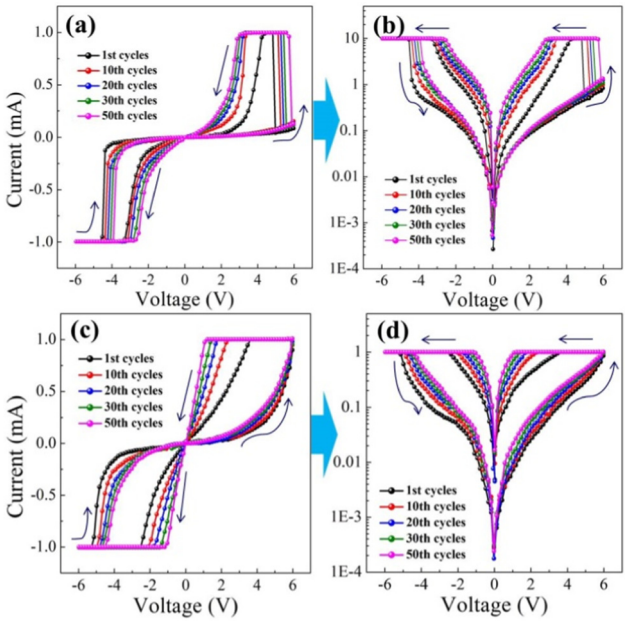

Fig. 6. (a) The I-V curves of continuous 50 cycles after the sample was annealed at 600 °C and then irradiated for 30 min. (b) The corresponding I-V curves in the logarithmic form. (c) The I-V curves of continuous 50 cycles after the sample annealed at 600 °C and then irradiated for 45 min. (d) The corresponding I-V curves in the logarithmic form.

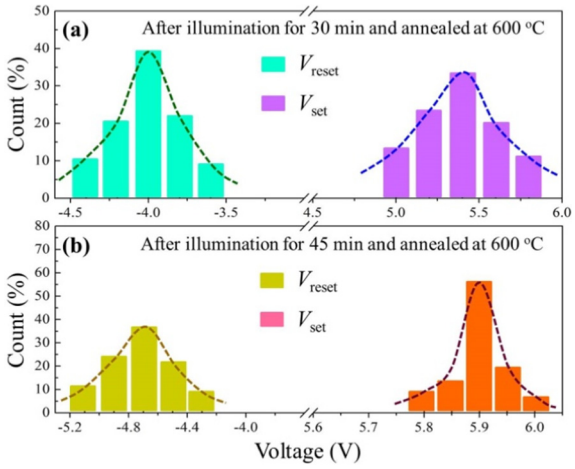

Fig. 7. The range of V_{set} and V_{rest} voltages, and the fitting curve is satisfied the Gaussian distribution. (a) The sample was firstly annealed at 600 °C and then irradiated for 30 min. (b) The sample was firstly annealed at 600 °C and then irradiated for 45 min.

is changed from −4.5 V to −3.5 V. Moreover, it is very obvious that the fitting curve of V_{set} and V_{reset} voltages is satisfied the Gaussian distribution in Fig. 7(a).

Fig. 6(c) shows the I-V curves of continuous 50 cycles after the sample was firstly annealed at 600 °C and then irradiated for 45 min, in which we can see that the loop is also continuously increased with the cycle times. The corresponding I-V curves in the logarithmic form are exhibited in Fig. 6(d), and we can find the range of V_{set} voltage is from 5.77 V to 6.25 V from Fig. 7(b), and the V_{rest} voltage is changed from −5.2 V to −4.19 V. Moreover, it is very obvious that the fitting curve of V_{set} and V_{reset} voltages is also satisfied the Gaussian distribution in Fig. 7(b).

The distribution of high resistance state (HRS) and low resistance state (LRS) is shown in Fig. 8. It can be observed that the

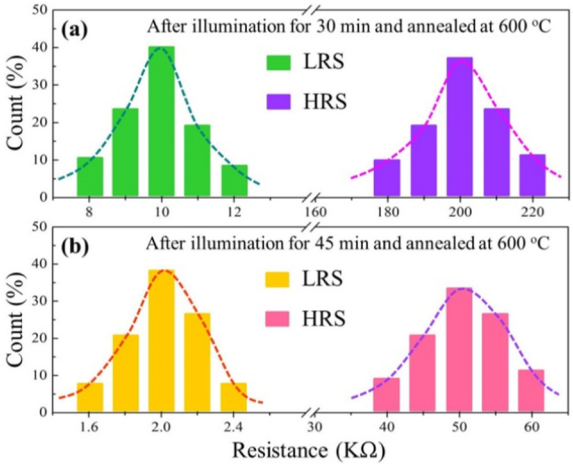

Fig. 8. The distribution of HRS and LRS. (a) After light-illumination for 30 min and annealed at 600 °C; (b) after light-illumination for 45 min and annealed at 600 °C.

maximum probability value of LRS is ~10 KΩ but it is ~200 KΩ at HRS for the device after illumination for 30 min under annealed at 600 °C. In other word, the HRS/LRS resistance ratio can reach ~20. Fortunately, the HRS/LRS resistance ratio can be increased to ~25 for the device after illumination for 45 min under annealed at 600 °C. The larger memory window can provide a more high-discriminate logical statement for storage information [31]. However, we can observe that the device shows obvious attenuation when the cycle times exceeds 200 cycles or retention testing over 103 s for the 600 °C annealed device irradiated for 30 min (Fig. 9), which may be due to the Joule heat generated in the material with increasing of the testing time, resulting in the gradual degradation of device performance.

Fig. 10(a) and (b) show the I–V curves on a log–log scale when the sample was annealed at 600 °C and then irradiated for 30 min, in which these scatters are experimental data and the straight lines are the theoretically fitting curves. We can see that the slope is ~1.12 in the low voltage for positive voltage region and it is ~0.87 in the negative voltage region. With the increasing of applied voltage, the slope is also increased to ~2.21. However, in the Fig. 10(c) and (d), the I–V curves on a log–log scale for the sample irradiated for 45 min and annealed at 600 °C exhibit similar electrical conductivity. The slope in the low voltage region is around ~1.0, which indicates an Ohmic conductance in the low voltage region [32]. With the increasing of applied voltage, the

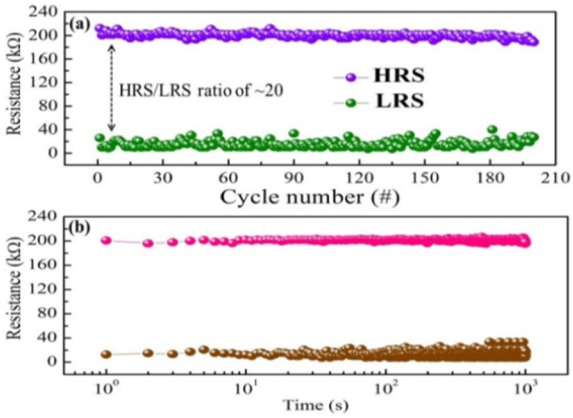

Fig. 9. The cycles testing and retention testing for 600 °C annealed sample under light-illumination for 30 min.

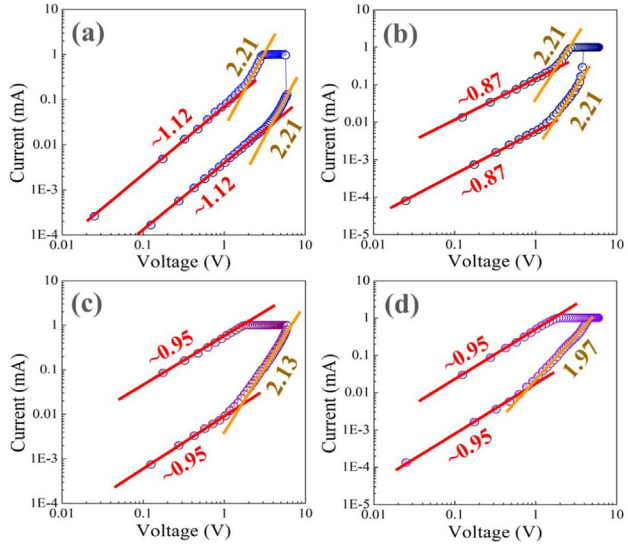

Fig. 10. (a) and (b) I–V curves on a log–log scale for the sample annealed at 600 °C and then irradiated for 30 min. (c) and (d) I–V curves on a log–log scale for the sample annealed at 600 °C and then irradiated for 45 min. These scatters are experimental data and these straight lines are the fitting curves from the theoretical models.

slope of I-V curve can reach ~2.13, ~2.21 and ~1.97, respectively, indicating the relation of $I \propto V^m$, the corresponding conductive mechanism depends on the classical trap-controlled space charge limited conduction (SCLC) [33]. It seems that the charge transfer happens between the top electrode ITO and the active layers of WO_3 film in the charge limited region [34]. For this device, the photo-generated carrier-regulated SCLC space should be responsible for the light-controlled resistive switching performances, which can be appropriately described by the Eq. (1) [35]:

$$J \propto \frac{V^{m+1}}{d^{2m+1}} \tag{1}$$

where the J is the current density, the V is the applied voltage, the d is the thickness of the functional layer, and the m is the fitting index. When $m = 0$, the I-V characteristic comply Ohmic law ($I \propto V$), when $m = 1$, which means Child's square law ($I \propto V^2$) happened, when $m = 2$, the current slope rise ($I \propto V^x$, $x > 2$) with a high field, which is described by Eq. (2) [36,37]:

$$J \propto \frac{9}{8}\varepsilon_i \mu \frac{V^2}{d^3} \tag{2}$$

Here the J is the current density, the ε_i is the permittivity of the oxide, the μ is the mobility, and the d is thickness of functional layer.

In order to clarify the physical mechanism of resistance switching effect in the ITO/WO_3/AZO device, the WO_3 films were characterized by ultraviolet–visible spectrophotometer, and the corresponding ultraviolet–visible absorption spectra are shown in Fig. 11(a). It can be confirmed that WO_3 films have significant light absorption in the visible region (400 nm ~ 760 nm). When the photon energy absorbed by the electron is larger than the bandgap, the excitation of the electron-hole pair will cause the movement of the photogenerated carriers, that is, the carriers are directly excited from the ground state of the bandgap to the conduction band. It is well known that the Fermi levels of ITO, WO_3 and AZO are different, as shown in Fig. 11(b). When they are in contact with each other, the interface will form a Schottky barrier [38,39]. When an external voltage is applied to the top electrode ITO and bottom electrode AZO, the movement of carriers will be limited near the interface, and the Schottky barrier region is equivalent to a tunnel gap [40], as shown in Fig. 11(c). In other words, a charge-limited

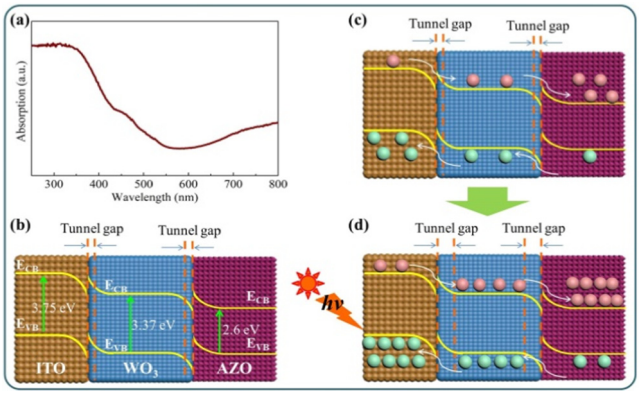

Fig. 11. (a) The ultraviolet–visible absorption spectra of WO_3 film. (b) Energy band structure of ITO, WO3 and AZO, respectively. The schematic diagram of migration of carriers and the formation of interface tunnel gap at dark (c) and under light-illumination (d), respectively.

region will be formed at the two interfaces of ITO/WO_3 and WO_3/AZO, leading to an internal electric field would be formed in a charge-limited region, and its direction is opposite to that of the external electric field. Therefore, to a certain extent, it prevents the transmission of electric charge in these interfaces [41].

When the device is exposed in light-illumination, these electrons at the valence band level would absorb photons and then transit to its conduction band [42,43], as shown in Fig. 11(d), making it become a free-moving charge which is called photogenerated carriers [44]. Because a large number of photogenerated carriers can be generated after the device is light-illuminated, more electrons and holes are accumulated in the confined charge region [45]. As a result, the height of Schottky barrier increases continuously, which corresponds to the broadening of tunnel gap, and more carriers are accumulated at the interface, leading to an enhanced resistance switching effect [46,47]. Therefore, our observed enhanced resistive switching memory behaviour in ITO/WO_3/AZO device originates from more photogenerated carriers generated after the device was exposed to light-illumination.

4. Conclusions

To summary, a resistive switching memory device with ITO/WO_3/AZO structure was prepared by magnetron sputtering. An enhanced memory behavior is observed when the sample was firstly annealed 600 °C and then illuminated for 45 min, and the V_{set} and V_{reset} voltages are also increased, which is accompanied by the HRS/LRS resistance ratio increased to ~25 for illumination time of ~45 min for 600 °C annealed sample. Finally, a physical model on the tunnelling of photon-generated carrier in the Schottky barrier layer driven by electric pulse is suggested to explain the enhanced resistive switching memory behavior. In particular, the proposed mechanism is highly pivotal for the resistive switching phenomenon to be properly applied in the nonvolatile RRAM devices by adding photo-control as an additional control means associated with the electrical pulse for multistate memory application in future.

Acknowledgements

This work was supported by the National Key Research and Development Plan (No. SQ2017YFE030073).

References

[1] A. Sawa, Resistive switching in transition metal oxides, Mater. Today 11 (2008) 28–36.

[2] F. Zhang, H. Zhang, S. Krylyuk, C.A. Milligan, Y. Zhu, D.Y. Zemlyanov, L.A. Bendersky, B.P. Burton, A.V. Davydov, J. Appenzeller, Electric-field induced structural transition in vertical $MoTe_2$-and $Mo_{1-x}W_xTe_2$-based resistive memories, Nat. Mater. 18 (2019) 55–61.

[3] Z. Lv, Q. Hu, Z.X. Xu, J. Wang, Z. Chen, Y. Wang, M. Chen, K. Zhou, Y. Zhou, S.T. Han, Organic memristor utilizing copper phthalocyanine nanowires with infrared response and cation regulating properties, Adv. Electron. Mater. 4 (2019) 1800793.

[4] H.J. Kim, T.H. Park, K.J. Yoon, W.M. Seong, J.W. Jeon, Y.J. Kwon, Y. Kim, D.E. Kwon, G.S. Kim, T.J. Ha, S.G. Kim, J.H. Yoon, C.S. Hwang, Fabrication of a Cu-cone-shaped cation source inserted conductive bridge random access memory and its improved switching reliability, Adv. Funct. Mater. 3 (2019) 1806278.

[5] S. Gao, X. Yi, J. Shang, G. Liu, R.W. Li, Organic and hybrid resistive switching materials and devices, Chem. Soc. Rev. 48 (2019) 1531–1565.

[6] N. Han, M.U. Park, K.H. Yoo, Memristive switching in $Bi_{1-x}Sb_x$ nanowires, ACS Appl. Mater. Interfaces 8 (2016) 9224–9230.

[7] Y. Wang, J. Yang, Z. Wang, J. Chen, Q. Yang, Z. Lv, Y. Zhou, Y. Zhai, Z. Li, S.-T. Han, Near-infrared annihilation of conductive filaments in quasiplane MoSe2/Bi2Se3 nanosheets for mimicking heterosynaptic plasticity, Small 15 (2019) 1805431.

[8] F. Alibart, L. Gao, B.D. Hoskins, D.B. Strukov, High precision tuning of state for memristive devices by adaptable variation-tolerant algorithm, Nanotechnology 23 (2012) 075201.

[9] Z. Wang, L. Wang, M. Nagai, L. Xie, M. Yi, W. Huang, Nanoionics-enabled memristive devices: Strategies and materials for neuromorphic applications, Adv. Electr. Mater. 3 (2017) 1600510.

[10] Y. Shi, X. Liang, B. Yuan, V. Chen, H. Li, F. Hui, Z. Yu, F. Yuan, E. Pop, H.-S. Philip Wong, M. Lanza, Electronic synapses made of layered two-dimensional materials, Nat. Electr. 1 (2018) 458–465.

[11] M.D. Pickett, J. Borghetti, J.J. Yang, G. Medeiros-Ribeiro, R.S. Williams, Coexistence of memristance and negative differential resistance in a nanoscale metal-oxide-metal system, Adv. Mater. 23 (2011) 1730–1733.

[12] B. Sun, W. Zhao, L. Wei, H. Li, P. Chen, Enhanced resistive switching effect upon illumination in self-assembled $NiWO_4$ nano-nests, Chem. Commun. 50 (2014) 13142–13145.

[13] B. Sun, L. Wei, H. Li, X. Jia, J. Wu, P. Chen, The DNA strand assisted conductive filament mechanism for improved resistive switching memory, J. Mater. Chem. C 3 (2015) 12149–12155.

[14] Y.J. Jeong, J. Lee, J. Moon, J.H. Shin, W.D. Lu, *K*-means data clustering with memristor networks, Nano Lett. 18 (2018) 4447–4453.

[15] H. Al-Bustami, G. Koplovitz, D. Primc, S. Yochelis, E. Capua, D. Porath, R. Naaman, Y. Paltiel, Single nanoparticle magnetic spin memristor, Small 14 (2018) 1801249.

[16] B. Sun, M. Tang, J. Gao, C.M. Li, Light-controlled simultaneous resistive and ferroelectricity switching effects of $BiFeO_3$ film for a flexible multistate high-storage memory device, ChemElectroChem 3 (2016) 896–901.

[17] S. Chen, Z. Lou, D. Chen, G. Shen, An artificial flexible visual memory system based on an UV-motivated memristor, Adv. Mater. 30 (2018) 1705400.

[18] S. Xie, L. Pei, M. Li, Y. Zhu, X. Cheng, H. Ding, R. Xiong, Light-controlled resistive switching and voltage-controlled photoresponse characteristics in the Pt/CeO_2/Nb:$SrTiO_3$ heterostructure, J. Alloys Comp. 778 (2019) 141–147.

[19] L. Lin, L. Liu, K. Musselman, G. Zou, W.W. Duley, Y.N. Zhou, Plasmonic-radiation-enhanced metal oxide nanowire heterojunctions for controllable multilevel memory, Adv. Funct. Mater. 26 (2016) 5979–5986.

[20] B. Sun, Y. Liu, W. Zhao, J. Wu, P. Chen, Hydrothermal preparation and white-light-controlled resistive switching behavior of BaW_O4 nanospheres, Nano-Micro Lett. 7 (2015) 80–85.

[21] M. Ungureanu, R. Zazpe, F. Golmar, P. Stoliar, R. Llopis, F. Casanova, L.E. Hueso, A light-controlled resistive switching memory, Adv. Mater. 24 (2012) 2496–2500.

[22] L. Wang, K.J. Jin, C. Ge, C. Wang, H.Z. Guo, H.B. Lu, G.Z. Yang, Electro-photo double modulation on the resistive switching behavior and switchable photoelectric effect in $BiFeO_3$ films, Appl. Phys. Lett. 102 (2013) 252907.

[23] S.K. Deb, Opportunities and challenges in science and technology of WO_3 for electrochromic and related applications, Solar Energy Mater. Solar Cells 92 (2008) 245–258.

[24] G. Wang, Y. Ling, H. Wang, X. Yang, C. Wang, J.Z. Zhang, Y. Li, Hydrogen-treated WO_3 nanoflakes show enhanced photostability, Energy Environ. Sci. 5 (2012) 6180–6187.

[25] S.-H. Lee, R. Deshpande, P.A. Parilla, K.M. Jones, B. To, A.H. Mahan, A.C. Dillon, Crystalline WO_3 nanoparticles for highly improved electrochromic applications, Adv. Mat. 18 (2006) 763–766.

[26] X.-L. Li, T.-J. Lou, X.-M. Sun, Y.-D. Li, Highly sensitive WO_3 hollow-sphere gas sensors, Inorg. Chem. 43 (2004) 5442–5449.

[27] W. Li, P. Da, Y. Zhang, Y. Wang, X. Lin, X. Gong, G. Zheng, WO_3 nanoflakes for enhanced photoelectrochemical conversion, ACS Nano 8 (2014) 11770–11777.

[28] S.M. Yong, T. Nikolay, B.T. Ahn, D.K. Kim, One-dimensional WO_3 nanorods as photoelectrodes for dye-sensitized solar cells, J. Alloys Comp. 547 (2013) 113–117.

[29] P. Zheng, B. Sun, Y. Chen, H. Elshekh, T. Yu, S. Mao, S. Zhu, H. Wang, Y. Zhao, Z. Yu, Photo-induced negative differential resistance in a resistive switching memory device based on $BiFeO_3$/ZnO heterojunctions, Appl. Mater. Today 14 (2019) 21–28.

[30] B. Sun, Y. Liu, W. Zhao, P. Chen, Magnetic-field and white-light controlled resistive switching behaviors in Ag/[$BiFeO_3$/γ-Fe_2O_3]/FTO device, RSC Adv. 5 (2015) 13513–13518.

[31] G. Zhou, S. Duan, P. Li, B. Sun, B. Wu, Y. Yao, X. Yang, J. Han, J. Wu, G. Wang, L. Liao, C. Lin, W. Hu, C. Xu, D. Liu, T. Chen, L. Chen, A. Zhou, Q. Song, Coexistence of negative differential resistance and resistive switching memory at room temperature in TiOx modulated by moisture, Adv. Electr. Mater. 3 (2018) 1700567.

[32] H. Wang, F. Meng, Y. Cai, L. Zheng, Y. Li, Y. Liu, Y. Jiang, X. Wang, X. Chen, Sericin for resistance switching device with multilevel nonvolatile memory, Adv. Mater. 25 (2013) 5498–5503.

[33] G. Chen, C. Song, C. Chen, S. Gao, F. Zeng, F. Pan, Resistive switching and magnetic modulation in cobalt-doped ZnO, Adv. Mater. 24 (2012) 3515–3520.

[34] Y. Wang, Z. Lv, Q. Liao, H. Shan, J. Chen, Y. Zhou, L. Zhou, X. Chen, V.A.L. Roy, Z. Wang, Z. Xu, Y.J. Zeng, S.T. Han, Synergies of electrochemical metallization and valance change in all-inorganic perovskite quantum dots for resistive switching, Adv. Mater. 30 (2018) 1800327.

[35] P. Han, B. Sun, S. Cheng, F. Yu, B. Jiao, Q. Wu, Preparation of MoSe2 nano-islands array embedded in a TiO_2 matrix for photo-regulated resistive switching memory, J. Alloys Comp. 664 (2016) 619–625.

[36] G. Zhou, B. Sun, Y. Yao, H. Zhang, A. Zhou, K. Alameh, B. Ding, Q. Song, Investigation of the behaviour of electronic resistive switching memory based on $MoSe_2$-doped ultralong Se microwires, Appl. Phys. Lett. 109 (2016) 143904.

[37] P. Han, B. Sun, J. Li, T.J. Li, Q.L. Shi, B.X. Jiao, Q.S. Wu, X.J. Zhang, Ag filament induced nonvolatile resistive switching memory behaviour in hexagonal $MoSe_2$ nanosheets, J. Colloid Interface Sci. 505 (2017) 148–153.

[38] P. Zheng, B. Sun, Y. Zhao, Z. Yu, Tunneling of carrier at the interface barrier induced nonvolatile resistive switching memory behaviors, Mater. Today Commun. 16 (2018) 164–168.

[39] T. Guo, B. Sun, Z. Yu, H. Zhao, M. Lei, Y. Zhao, Overwhelming coexistence of negative differential resistance effect and RRAM, Phys. Chem. Chem. Phys. 20 (2018) 20635–20640.

[40] G. Zhu, Y. Yao, X. Zhao, X. Liu, B. Sun, A. Zhou, Band gap energies for white nanosheets/yellow nanoislands/purple nanorods of CeO_2, RSC Adv. 6 (2016) 59370–59374.

[41] J. Zhao, M. Zhang, S. Wan, Z. Yang, C.S. Hwang, Highly flexible resistive switching memory based on the electronic switching mechanism in the Al/TiO_2/Al/polyimide structure, ACS Appl. Mater. Interfaces 10 (2018) 1828–1835.

[42] Y. Cui, W. Liu, R. Wang, Visible light initiated and collapsed resistive switching in $TbMnO_3$/Nb:$SrTiO_3$ heterojunctions, Phys. Chem. Chem. Phys. 15 (2013) 6804–6808.

[43] T.L. Qu, Y.G. Zhao, D. Xie, J.P. Shi, Q.P. Chen, T.L. Ren, Resistance switching and white-light photovoltaic effects in BiFeO3/Nb-$SrTiO_3$ heterojunctions, Appl. Phys. Lett. 98 (2011) 173507.

[44] E. Yoo, M. Lyu, J.H. Yun, C. Kang, Y. Choi, L. Wang, Bifunctional resistive switching behavior in an organolead halide perovskite based Ag/$CH_3NH_3PbI_{3-x}Cl_x$/FTO structure, J. Mater. Chem. C 4 (2016) 7824–7830.

[45] Z. Lv, Y. Wang, Z. Chen, L. Sun, J. Wang, M. Chen, Z. Xu, Q. Liao, L. Zhou, X. Chen, J. Li, K. Zhou, Y. Zhou, Y.J. Zeng, S.-T. Han, Vellaisamy.A.L. Roy, Phototunable biomemory based on light-mediated charge trap, Adv. Sci. 5 (2018) 1800714.

[46] H. Tan, G. Liu, X. Zhu, H. Yang, B. Chen, X. Chen, J. Shang, W.D. Lu, Y. Wu, R.W. Li, An optoelectronic resistive switching memory with integrated demodulating and arithmetic functions, Adv. Mater. 27 (2015) 2797–2803.

[47] L. Zhang, J. Chen, J. Cao, D. He, X. Xing, Large resistive switching and switchable photovoltaic response in ferroelectric doped $BiFeO_3$-based thin films by chemical solution deposition, J. Mater. Chem. C 3 (2015) 4706–4712.